Sensors & Actuators: B. Chemical 305 (2020) 127423

Contents lists available at ScienceDirect

Sensors and Actuators B: Chemical

journal homepage: www.elsevier.com/locate/snb

An ammonia sensor composed of polypyrrole synthesized on reduced graphene oxide by electropolymerization

Xiaohui Tang[a,*], Jean-Pierre Raskin[a], Nadzeya Kryvutsa[b], Sophie Hermans[b], Oleksandr Slobodian[c], Alexei N. Nazarov[c], Marc Debliquy[d]

[a] ICTEAM Institute, Université catholique de Louvain (UCLouvain), Place du Levant, 3, 1348 Louvain-la-Neuve, Belgium
[b] IMCN Institute, Université catholique de Louvain (UCLouvain), Place L. Pasteur 1, 1348 Louvain-la-Neuve, Belgium
[c] Alexei N. Nazarov, Lashkaryov Institute of Semiconductor Physics NAS of Ukraine Kyiv, Ukraine
[d] Materials Science Department, University of Mons, 7000 Mons, Belgium

ARTICLE INFO

Keywords:
Reduced graphene oxide
Polypyrrole
Electropolymerization
Ammonia sensor

ABSTRACT

We report an ammonia (NH_3) sensor in which a ultrathin polypyrrole (PPy) layer is synthesized on reduced graphene oxide (rGO) by electropolymerization. The PPy/rGO composite is characterized by scanning electron microscopy, secondary ion mass spectrometry, Raman spectroscopy, and X-ray photoelectron spectroscopy. The sensor exhibits an excellent performance in the selective sensing of NH_3 at room temperature, having a high, fast, reversible and linear response. These performances are attributed to the synergistic effect of the ultrathin PPy layer and rGO. Specifically, NH_3 molecules are adsorbed on the ultrathin PPy layer, electrons transfer from NH_3 to the PPy layer, changing the PPy layer resistance. The ultrathin PPy layer over rGO allows NH_3 molecules to pass through and react with sp^2-bonded carbon atoms, also changing the rGO resistance. Moreover, the rGO sheets are not only a support material for the ultrathin PPy electropolymerization but also provide an efficient pathway for electron transfer, thereby, accelerating the sensor response and recovery. Meanwhile, the ultrathin PPy layer plays an important role in the sensor selectivity and immunity to humidity. Our research indicates that the post-step PPy electropolymerization is very promising for sensor fabrication and compatible with CMOS technology. These make it possible to design and manufacture the PPy/rGO sensors with integrated circuits onto the same Si wafer for different applications. Importantly, the fabrication method of the present sensor is easy and low cost. Therefore it is regarded as being scalable for mass production of NH_3 sensors.

1. Introduction

Ammonia (NH_3) is one of the most harmful pollutant gases. Most of NH_3 is emitted from electronic manufacturing, chemical industries, medical treatment, and human activities [1,2]. NH_3 can give rise to severe problems for human health: stimulating eyes, skin and respiratory tract even if present at a very low concentration and causing damage to kidneys, lung, liver or even death with a large amount of inhalation [3]. The TLV-STEL (Threshold Limit Value-Short Term Exposure Limit) is 35 ppm. It is crucial to timely detect NH_3 by using practical methods. NH_3 detection technology is roughly catalogued into spectrum analysis (such as, absorption, chromatography, photoacoustic and laser-coupled spectroscopies) and gas sensors [4–6]. Although the former is ultrasensitive at concentrations down to 1 ppb, it needs a long and complicated analysis cycle [7–9]. The gas sensors are suitable for on-site detection. NH_3 sensors have been broadly used in environment monitoring, agricultural and industrial fields [10,11]. Recently, they have found a new application in medical field. Specifically, NH_3 sensors can non-invasively diagnose many diseases (for example, ulcers, hepatic injury, renal disorders and cancers) through detecting NH_3 concentration from human breath [12–14].

The most typical materials used for NH_3 sensing are metal oxides, such as WO_3, ZnO, In_2O_3, SnO_2, TiO_2 and so on. These materials exhibit a detection limit as low as 1 ppm, but they suffer from poor selectivity. In addition, they operate at high temperatures (100–450 °C), leading to large power consumption, safety hazard, short lifetime and high cost [15–17]. Therefore, it is important to develop NH_3 sensors with high performance and room-temperature operation by using economic sensing materials and simple fabrication technology.

Presently, graphene (G) is being researched and developed as a sensing material because of (i) single-layer graphene exposes all carbon atoms to environment, providing the largest number of binding sites per

* Corresponding author.
E-mail address: xiaohui.tang@uclouvain.be (X. Tang).

https://doi.org/10.1016/j.snb.2019.127423
Received 16 July 2019; Received in revised form 13 November 2019; Accepted 14 November 2019
Available online 19 November 2019
0925-4005/ © 2019 Elsevier B.V. All rights reserved.

unit volume and (ii) high-quality crystal lattice and the high carrier mobility of graphene inherently ensures low electrical noise and low power consumption. Therefore, one single adsorbed molecule causes a notable change in the resistance, allowing the sensing ability to one single molecule [18]. Generally, graphene can be obtained by chemical vapour deposition (CVD) on metal substrates, silicon sublimation from SiC substrate surface, or mechanical graphite exfoliation. The CVD yields large surface area of graphene sheets and its throughput is quite high. However, the CVD requires expensive equipment and high synthesis temperature. The issue of the epitaxial growth is to transfer graphene from the SiC substrate to target substrates. The exfoliation of graphite only provides small size of graphene foil. By contrast, reduced graphene oxide (rGO) can be converted from graphene oxide (GO) by thermal treatment or chemical reduction. The rGO synthesis is quite easy and cheap [19].

Some of NH_3 sensors fabricated from graphene-based materials have been exploited in the literature. Graphene is chemically inert and weakly binding with NH_3 molecules [9]. As a result, this requires a functionalization to generate a specific link between graphene and NH_3 molecules. Compared with graphene, reduced graphene oxide (rGO) is most beneficial for the NH_3 sensor fabrication because of its inherently structural defects and residual oxygen groups, namely C—OH, C—O—C and COOH. These structural defects and oxygen groups can provide an increased amount of binding sites and they are usually favourable for gas adsorption [20,21]. Particularly, rGO has great advantages of mass production and low cost [22–24]. The drawbacks of the rGO are poor selectivity, high Johnson noise and 1/f noise. However, recent published results have shown that the rGO electrical properties can be tuned by conducting polymers [25]. This provides a new route for the fabrication of NH_3 sensors from the rGO-based materials. The main conducting polymers with sensing function to NH_3 are polypyrrole (PPy) [26,27], polyaniline (PANI) [28,29] and their derivatives [30]. They present inexpensive cost, environmental stability and friendly, acceptable conductance, room-temperature operation, reversible doping chemistry and simple synthesis. Moreover, both PPy and PANI are compatible with rGO.

Recently, we have reported a fast and room-temperature operation NH_3 sensor [31]. The sensing material of the sensor is composed of an ultrathin PPy layer synthesized on CVD graphene by electropolymerization. Our previous results indicate that the combination of these two materials significantly improves the sensor performance. To reduce the cost of the sensing material, simplify the process of the sensor fabrication, and increase the throughput of the sensor production, here we develop a cost-effectiveness and room-temperature operating HN_3 sensor, in which the expensive CVD graphene is replaced by the cheap rGO. Hereafter, this sensor is referred to as the PPy/rGO sensor. Although some of PPy/rGO sensors have been reported in the literature (see Table 1), all of the PPy syntheses are based on chemical methods, or rGO is randomly introduced in polypyrrole sheets. It is the first time that the rGO is used as the support material for the PPy synthesis in electropolymerization. Thicker polymer shows high sensitivity and slow response, while thinner one exhibits fast response and low sensitivity. A trade-off between the sensitivity and response time should be considered. The PPy thickness can be well controlled to 20 nm in our process. This method is suitable for wafer-scale production of the sensor and compatible with CMOS technology. Compared with the previous PPy/G sensor, the fabrication method of the PPy/rGO sensor is much easier and cheaper. It is emphasized that the PPy/rGO sensor demonstrates some performances better over the PPy/G sensor. Table 1 summarizes recently published NH_3 sensors based on PPy, PANI and rGO, their compounds, and related materials, operating at room temperature. For the purpose of comparison, the key parameters of our sensors (the PPy/G and PPy/rGO sensors) are also summarized in Table 1. Following the synthesis, the PPy/rGO composite is characterized by scanning electron microscopy (SEM), secondary ion mass spectrometry (SIMS), Raman, and X-ray photoelectron spectroscopy (XPS).

2. Materials and methods

2.1. Fabrication of the PPy/rGO sensor

The fabrication process of the PPy/rGO sensor includes three simple steps: (i) the preparation of the interdigitated area electrodes (IDEs) by standard microfabrication process; (ii) the GO deposition by ultrasonic spray pyrolysis technique and the GO thermal reduction; and (iii) the ultrathin PPy layer synthesis by electropolymerization.

A 3-inch Si wafer is used as a starting substrate. 90-nm-thick SiO_2 is thermally grown on the substrate for insulating the Si substrate. The wafer is spin coated with photoresist to define the IDEs on the SiO_2/Si substrate. The surface area of the sensing is designed to 200 × 200 μm^2. The finger width and gap width are 5 μm and 2 μm, respectively. Ti and Au layers with thicknesses of 5 and 50 nm are successively deposited onto photoresist. The wafer is then soaked with acetone for removing photoresist in lift-off process. As a result, the IDEs are predefined on the wafer (see Fig. 1a). The 3-inch Si wafer is cut into many dies with an area of 3 × 6 mm^2 (see Fig. 1b). Each die includes a pair of IDEs.

The stable GO dispersions (in water) with a concentration of 4 mg/mL are purchased from Sigma Aldrich, NV. The GO dispersions are deposited on the IDEs by ultrasonic spray pyrolysis technique (Fig. 1c) and slowly dried at room temperature for a few hours. The details of ultrasonic spray pyrolysis can be found in our previous work [44,45]. We test 3 methods for depositing the GO dispersions: dropping, spraying, and ultrasonic spray pyrolysis. The results indicate that the last one provides a quite thin GO layer on the IDEs (see Supplementary material). This guarantees the complete coverage of the PPy polymer in the following electropolymerization. Then the GO is reduced to rGO by heating at 300 °C for 15 min in nitrogen. The die with the rGO on the IDEs is glued and wire-bonded in a 24 pin dual-inline package (see Fig. 1d). The package can be contacted with our smart prototype [31], which can directly demonstrate the NH_3 concentrations on a liquid-crystal display and also transmit the measured data to a computer for the analysis.

In this study, we use the same synthesis setup and conditions as described in [31] for the PPy electropolymerization. The unique change is the CVD graphene replaced by the rGO. It is the first time that the rGO is used as the support material for the PPy synthesis in electropolymerization. The electropolymerization is carried out in a solution bath consisting of 0.35 mL pyrrole, 0.6 g $NaClO_4$ and 50 mL acetonitrile at 20 °C. The package mentioned above is immersed in the solution bath, where the rGO on the IDEs is used as the working electrode. The counter and reference electrodes are made of Pt and Ag/AgCl, respectively. When a voltage pulse of 0.9 V is applied to the working electrode for 2 cycles, an ultrathin PPy layer with a thickness of about 20 nm is formed on the rGO sheets. After the electropolymerization, the dies are washed with ethanol. The analysis samples, in which the PPy/rGO is directly deposited on the SiO_2/Si substrate, are prepared by using the same process for physical characterization. We also prepare the naked rGO sensor without PPy for comparison. In this work, the PPy synthesis is performed after the wafer cutting and package bonding. For the wafer-scale production, this step can be done before the wafer cutting. In this case, the PPy layer can be simultaneously synthesized on many dies of one wafer.

It is important to point out that the fabrication of the PPy/rGO sensors shows the following advantages: (i) the PPy thickness can be well controlled to the nanometer scale by the number of voltage pulses, their duration and amplitude during the electropolymerization and the ultrathin PPy layer can be uniformly covered on the rGO surface; (ii) the sensing composite is based on cheap and easy-synthesis GO material so it avoids the transfer step of the CVD graphene (which is initially grown on metal substrates) and simplifies the procedures of the sensor fabrication; (iii) the post-step PPy electropolymerization is compatible

Table 1
Summary of recent research results for NH_3 sensors based on PPy, PANI and rGO, their compounds, and related materials, operating at room temperature.

Sensor type	GO reduction	Sensing materials	Synthesis method	Sensitivity	Detection limit	Response time	Recovery time	Ref.
Silver paste	Chemical Reduction	PPy/rGO	*in situ* COP	34.7 %/500 ppm	3 ppm	147 s	Heating at 50 °C	[32]
Chemiresistor	Chemical Reduction	PANI/rGO	*in situ* COP	344 %/100 ppm	10 ppm	20 s	27 s	[33]
IDEs	Chemical Reduction	Py-rGO	Py-vapour-reduced	22 %/100 ppm	5 ppb	134 s	310 s	[34]
IDEs	Chemical Reduction	Py-rGO/PANI	*in situ* P	14 %/1 ppm	0,2 ppm			[35]
IDEs	Chemical Reduction	Py-rGO	rGO mixed with P	2.4 %/1 ppb	1 ppb	1,4 s	76 s (IR)	[36]
IDEs	Chemical Reduction	PANI + rGO	*in situ* COP	37.1 %/50 ppm	20 ppm	18 min	2 min	[37]
IDEs	Chemical Reduction	rGO/G	CVD	2.88 %/0.5 ppm	36 ppb	150 s	325 s	[38]
Chemiresistor	Chemical Reduction	GO + Ag, Pt, Cu NPs	Metal salts	6.52 %/1 ppm	1.2, 1.6, 16 ppb	5 s	6 s	[39]
IDEs	Chemical Reduction	TiO_2/rGO	rGO mixed with TIP	1.7 %/ 10 ppm	5 ppm	114 s	304 s	[40]
IDEs	Heating 220 °C/2H	ZnO/rGO	Spraying process	3.05 %/50 ppm	10 ppm	84 s	216 s	[41]
IDEs	Heating 350 °C/3H	PANI/rGO-MnO_2	Mixing	59.2 %/50 ppm	5 ppm	18 min	4 min	[42]
3D	Hydrothermal 190 °C/ 14H	PPy/3D-rGO	chemical polymerization	3 %/ 1 ppm	330 ppb	5 s	20 s	[43]
Chemiresistor	CVD graphene	PPy/G	Electropolymerization	1.7 %/1 ppm	1 ppm	2 min	5 min	Previous work [31]
IDEs	GO Heating 300 °C/ 15min	PPy/rGO	Electropolymerization	6.1 %/1 ppm	< 1 ppm	1 min	5 min	This work

IDEs: interdigitated area electrodes, G: graphene, rGO: reduced graphene oxide, PPy: polypyrrole, PANI: polyaniline, COP: chemical oxidative polymerization, Py: pyrrole, P: polymerization, TIP: titanium isopropoxide, CVD: chemical vapour deposition, NPs: nanoparticles. The rest of the abbreviations can be found in the related references.

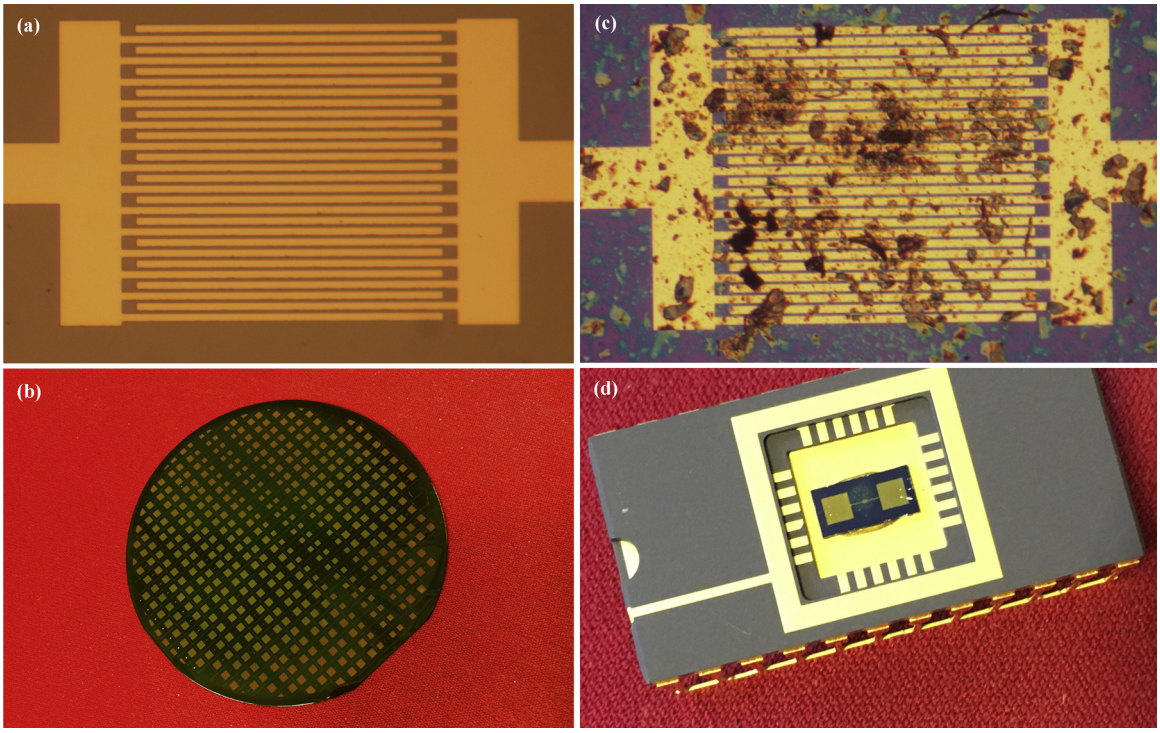


Fig. 1. Optical images: (a) a pair of interdigitated area electrodes (IDEs); (b) reduced graphene oxide deposited on the IDEs; (c) 3-inch Si wafer with IDEs; and (d) PPy/rGO bonded to 24 pin dual-in-line package.

with CMOS technology and suitable for mass production, making it possible to design and manufacture the PPy/rGO sensors with integrated circuits onto the same Si wafer for different applications in coming future; and (iv) the charge transfer process takes place at room temperature, the PPy/rGO sensors do not need heating element to operate at an elevated temperature with very low power consumption.

2.2. Measurements

The gaseous analytes are detected by measuring the resistance change of the sensor induced by adsorbing the target gas. The sensor response (S) is calculated by using the equation:

$$S = \frac{R_s - R_0}{R_0} = \frac{\Delta R}{R_0} \quad (1)$$

Where R_0 is the initial resistance and R_S is the maximum resistance upon exposure to the target gas. The response time t_{res} is defined as the time to reach 90 % of the total resistance change, whereas the recovery time t_{rec} refers to the time required for recovering the measured resistance to 90 % of its original value.

The detail of the measurement setup and smart prototype can be found in our previous work [31,46]. In brief, the sensor is placed in a sealed chamber with gas inlet and outlet ports. The current across the IDEs is provided by applying a constant voltage of 0.8 V. The sensor

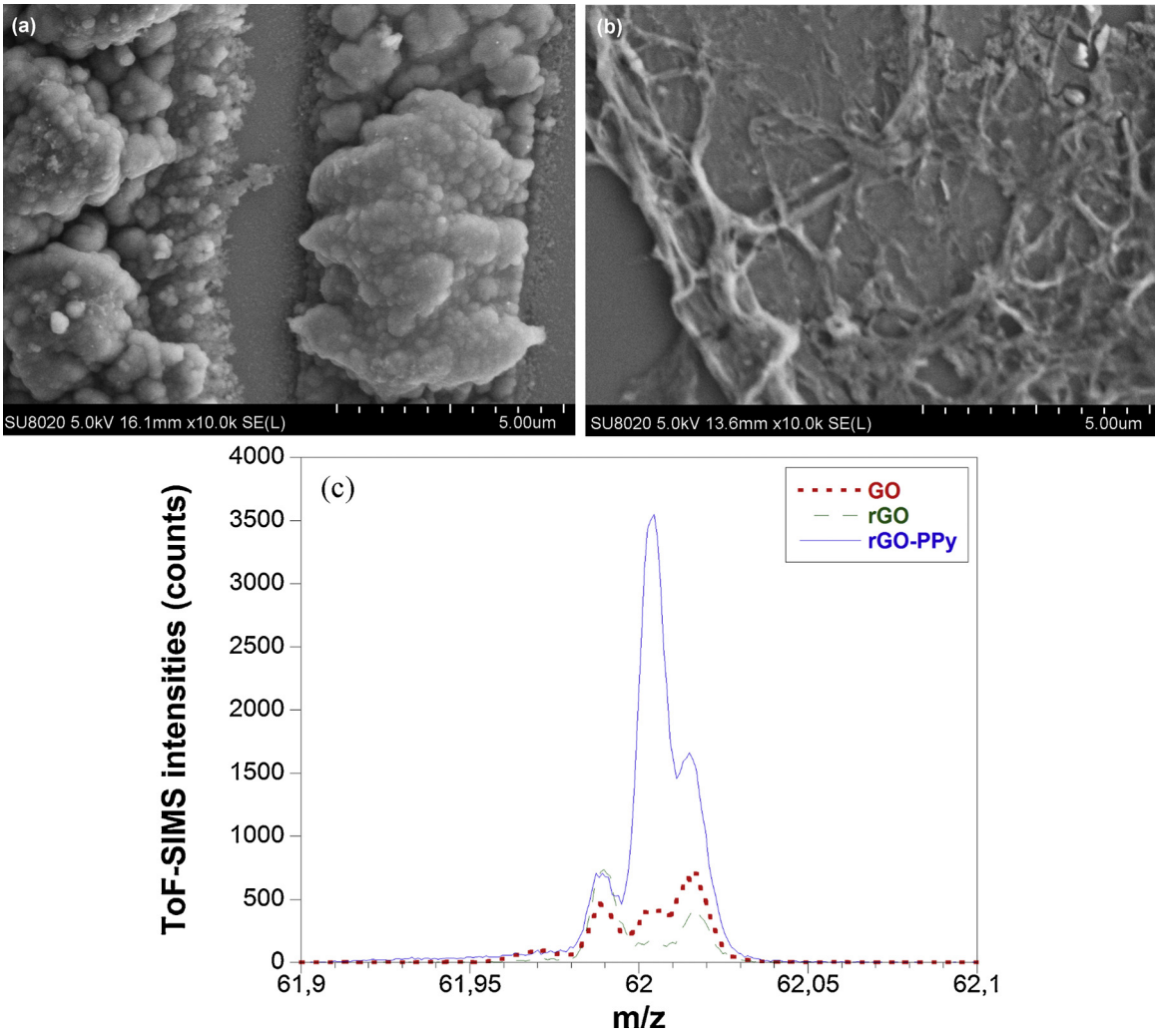


Fig. 2. Scanning electron microscopy top view of (a) the PPy; (b) the PPy/rOG composite and (c) ToF-SIMS mass spectra of the GO, the rGO and the PPy/rGO in the zone corresponding to the C_4N pyrrole molecular fragment.

resistance is measured by current-voltage characteristic in direct current mode. All the sensing measurements are carried out in real world environments, specifically at room temperature (20 °C), atmospheric pressure and wet air (relative humidity of 50 %), unless otherwise noted. Wet air and NH_3 are used as carrier gas and target gas, respectively. The concentration of commercial NH_3 is 100 ppm in a cylinder. The desired NH_3 concentration is obtained by diluting 100 ppm NH_3 with wet air. For example, for 1 ppm NH_3 concentration, we combine 10 mL/min of 100 ppm NH_3 in air with 490 mL/min of dry air and 500 mL/min of saturated wet air (100 % RH).

3. Results and discussion

3.1. Characterization

The morphology and structure of the pure PPy and PPy/rGO composite are characterized using scanning electron microscopy (SEM). The results are shown in Fig. 2a and b, respectively. The pure PPy shows cauliflower-like structure. For the PPy/rGO composite, an ultrathin PPy layer (about 20 nm) is grown on the rGO. As shown in Fig. 2a, the pure PPy layer is not thick enough to cover the insulated gap between the neighbouring electrodes. For passing current between the neighbouring electrodes, the PPy thickness should be further increased. However, the response and recovery of the thick PPy sensor are quite slow. Moreover, the thicker PPy can lead to cracks in the films, causing a loss of conductivity. These facts restrict the practical application of the thicker PPy. When the neighbouring electrodes are bridged by the rGO sheets, the PPy thickness can be decreased to 20 nm, thereby shorting the response and recovery times. In addition, the introduction of rGO improves the PPy conductance, reducing the sensor power consumption. These are clear advantages of the PPy/rGO sensor.

Chemical characterization of samples are carried out by using Time of Flight Secondary Ion Mass Spectrometry (ToF-SIMS), which provides molecular information by giving the mass of fragments extracted from the surface. Small pieces of Si/SiO_2 chips with GO, rGO or PPy/rOG coating are cut and fixed on the sample holder with double-sided adhesive tape. We perform 3 measurements at different locations. A ToF-SIMS instrument (IONTOF, GmbH, Münster, Germany) is used. A pulsed Bi_5^+ metal ion source is used to produce a primary beam using an acceleration voltage of 30 kV. An AC target current of 0.08 pA with a bunched pulse width shorter than 1 ns is used. Both positive and negative secondary ion species are analysed. For spectra, a raster of 128 × 128 data points over an area of 300 × 300 μm^2 is used. The total primary ion beam dose for each analysed area is always kept below 3×10^{10} ions. cm^{-2}, ensuring static conditions. Lateral resolution of ~ 3 μm and mass resolution $m/\Delta m > 7900$ at 62 m/z are maintained for positive and negative spectra acquisition. Charge compensation is done by interlaced electron flood gun (E_k = 20 eV). All data analyses are carried out using the software supplied by the instrument manufacturer, SurfaceLab (version 6.5).

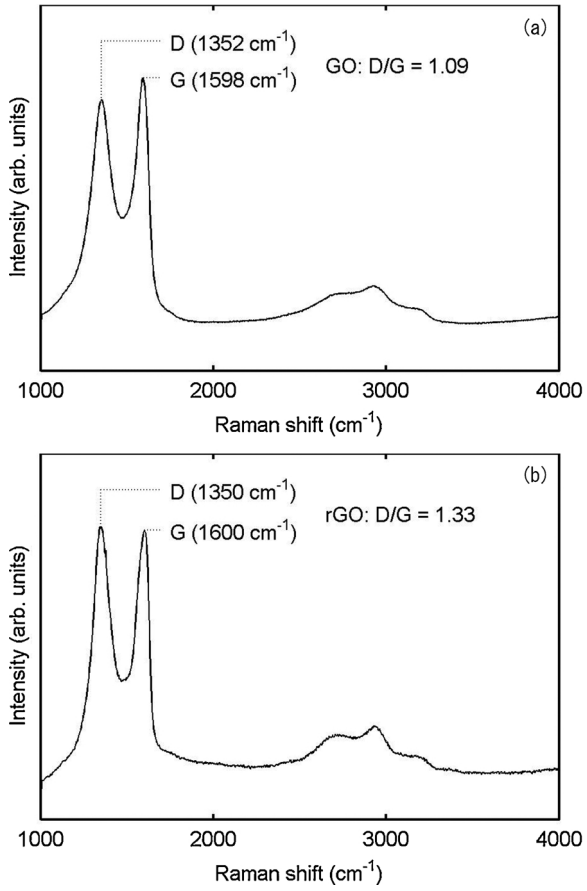


Fig. 3. Raman spectra: (a) for graphene oxide and (b) for reduced graphene oxide obtained by heating at 300 °C for 15 min.

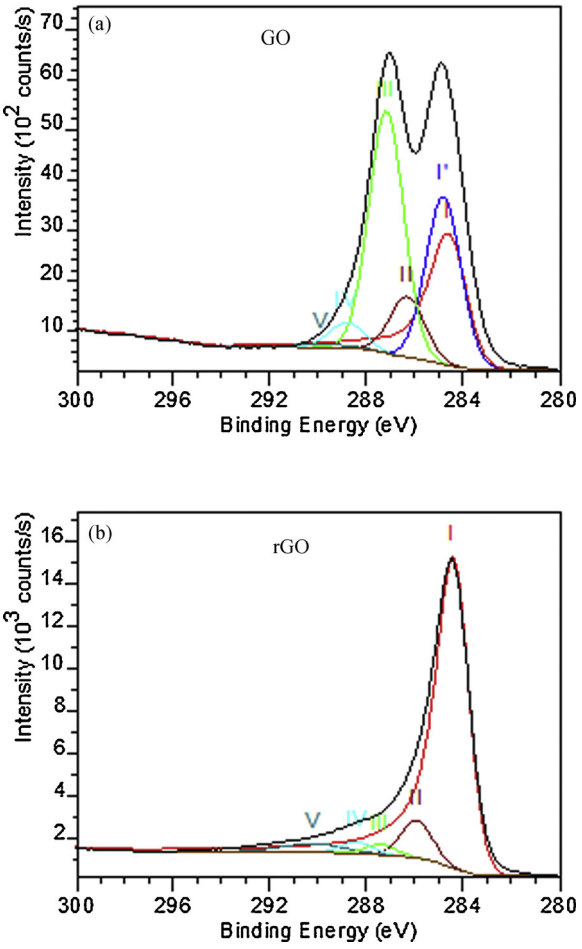


Fig. 4. X-ray photoelectron spectroscopy analysis of (a) GO and (b) rGO, in the C1s region, fitted with the following components: (I) **C**–(C,H) asymmetric contribution of graphitic carbon, (I') **C**– (C,H) symmetric contribution of non-aromatic carbon, (II) **C**–O, (III) **C**=O and O–**C**–O, (IV) O=**C**–O, (V) π→π* shake-up.

The three GO, rGO or PPy/rGO samples gave markedly different ToF-SIMS results. We analyse in particular C_xN_y fragments that are typical of the PPy polymer: the peaks at *m/z* values corresponding to CN, C_2N, C_2NH, C_3N, C_4N, C_4NH were observed in the PPy/rGO sample but are absent in the GO and rGO samples, confirming the presence of the PPy polymer coating. The C_4N molecular fragment in particular corresponds to one pyrrole unit (Fig. 2(c)) and is diagnostic of the macromolecular entity.

To verify the GO reduction, Micro-Raman measurements are performed by using a LabRam Horiba spectrometer (E_{Laser} = 514.5 nm). Fig. 3a shows a typical Raman spectrum of the GO. The D and G peaks are located at 1352 cm^{-1} and 1598 cm^{-1}, respectively. The D peak is associated with a defect-induced breathing mode of sp^2 rings [47,48], while the G peak originates from the first order scattering of the E_{2g} phonon of sp^2 C atoms [49]. The D/G intensity ratio of the GO is 1.09. After the GO reduction, the locations of both peaks almost unchanged as shown in Fig. 3b. However, the D/G intensity ratio increases from 1.09 to 1.33. This suggests forming more sp^2 domains [50] because the D/G intensity ratio is inversely proportional to the average size of the sp^2 clusters [51]. This implies that after GO reduction, new (or more) graphitic domains are formed and the sp^2 cluster number is increased [52]. The Raman results confirm that the heating conditions (at 300 °C for 15 min) have good reduction efficiency.

The reduction of the GO is further investigated by X-ray photoelectron spectroscopy (XPS). Fig. 4a and b present the C1s spectra for the GO and the rGO samples, respectively. The XPS analyses were carried out with a SSX 100/206 photoelectron spectrometer from Surface Science Instruments (USA), equipped with a monochromatized microfocus Al X-ray source (powered at 20 mA and 10 kV). Samples were stuck onto small holders with double-face adhesive tape and then placed on an insulating ceramic carousel (Macor®, Switzerland). The pressure in the analysis chamber was around 10^{-6} Pa. The angle between the surface normal and the axis of the analyser lens was 55°. The analysed area was approximately 1.4 mm^2 and the pass energy was set at 150 eV. Under these conditions, the full width measured at half maximum (FWHM) of the Au $4f_{7/2}$ peak for a clean gold standard sample was about 1.6 eV. A flood gun set at 8 eV and a Ni grid placed 1 mm above the sample surface were used for charge stabilisation. The binding energies were calculated with respect to the graphitic **C**–(C, H) component of the C1s peak fixed at 284.6 eV. Data treatment was performed with the CasaXPS program (Casa Software Ltd, UK), some spectra were decomposed with the least squares fitting routine provided by the software with a Gaussian/Lorentzian (85/15) product function and after subtraction of a non-linear baseline. The shape of the graphitic **C**–(C,H) component was adjusted with A(0.4,0.4,20) asymmetry parameter. Molar fractions were calculated using peak areas normalised based on acquisition parameters and sensitivity factors provided by the manufacturer.

Fig. 4 presents the XPS C1s spectra of the GO and rGO samples that have been fitted with six components. The first at lowest binding energy (BE) corresponds to carbon atoms in defect-free graphitic environment (**C**-(C,H)). It is followed at higher BEs by contributions from carbon atoms connected to oxygen atoms in **C**–O single, **C**=O double and O–**C**–O or O=**C**–O multiple bonds. The last peak is due to π→π* shake-up. It is noticeable that in the case of GO an additional

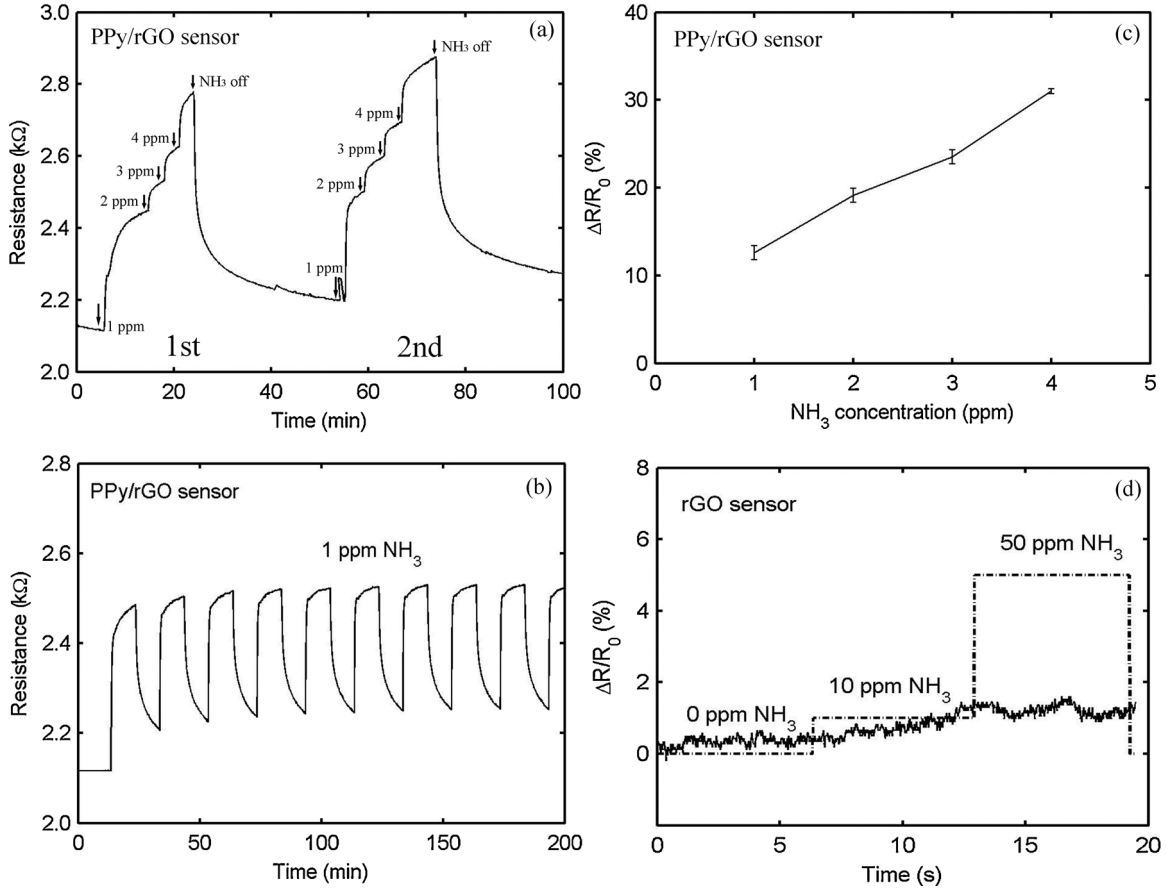


Fig. 5. Sensing behaviour of typical sensors at relative humidity of 50 % and at 20 °C: (a) the resistance of the PPy/rGO sensor exposed to NH_3 concentrations in a range from 1 to 4 ppm for 2 cycles; (b) the response of the PPy/rGO sensor exposed to 1 ppm NH_3 for 10 cycles; (c) the resistance of the PPy/rGO sensor as a function of NH_3 concentration; (d) the response of the naked rGO sensor exposed to NH_3 concentrations of 0, 10 and 50 ppm.

component is visible due to non-aromatic carbon atoms (**C**–(C,H)), together with much stronger contribution of carbon to oxygen **C**=O component. Compared with the GO sample, the intensities of the three C-O peaks in the rGO sample decrease markedly, indicating that GO has been successfully reduced to rGO with some amount of residual oxygenated surface groups after thermal treatment [53,54], which is also consistent with Raman results.

3.2. Sensor response

Fig. 5a shows the resistance behaviour of a typical PPy/rGO sensor exposed to NH_3 concentrations in a range from 1 to 4 ppm for 2 cycles. The resistance baseline of the sensor is 2114 Ohm in wet air (50% RH at 20 °C). The sensor resistance is increased with the NH_3 concentration. When NH_3 is switched off, the sensor resistance incompletely recovers to its original value due to the 'poisoning' effect of NH_3. However, the sensor can be rapidly recovered by annealing at 100 °C or short-time illumination. The sensor exposed to 10 cycles of 1 ppm NH_3 (see Fig. 5b) has a repeatable response of 12.6 ± 0.8 %. In this calculation, we exclude the data of the first cycle. Fig. 5c plots the sensor response as a function of the NH_3 concentration. A linear relationship can be observed in the range from 1 to 4 ppm. This simplifies the sensor calibration and benefits the sensor application. The sensor sensitivity is calculated to be 6.1 %/ppm by the slope of the linear curve. The response and recovery times of the PPy/rGO sensor are of 1 and 5 min, respectively, which are nearly the same as that in our previous PPy/G sensor. This is due to the same thickness of the PPy layer used for the PPy/G and PPy/rGO sensors. Fig. 5d shows the response of a naked rGO sensor. Compared to the PPy/rGO sensor, the naked rGO sensor exhibits noticeably lower response at room temperature. It needs the aid of the conducting polymer to improve its performance. In other words, the naked rGO has to be functionalized by the PPy layer.

3.3. Sensor selectivity

We expose the PPy/rGO sensor to CH_2O (formaldehyde). Fig. 6a shows the response of the PPy/rGO sensor for 15 ppm CH_2O. It can be seen that the sensor response is less than 2 % even at a CH_2O concentration of 15 ppm. Other interfering gas, such as H_2 (hydrogen), is also used for the evaluation. No response is observed (not shown here). It has been demonstrated in our previous work [55] that graphene is sensitive to H_2 only after functionalization (with Pd nano particles for instance). These facts confirm that the PPy/rGO sensor exhibits a good selective ability to NH_3 from certain interference gases, such as CH_2O and H_2.

When the PPy/rGO sensor is exposed to 1 ppm NO_2 (nitrogen dioxide), a response of about -12 % is observed as shown in Fig. 6b. This response is caused not only by the PPy itself but also by the rGO. NO_2 is a strong oxidizing gas that can accept electrons from PPy and rGO (the same phenomenon is observed in graphene). This increases the holes concentration, reducing the sensor resistance. As a result, the sign of the sensor response is negative. In the case of the simultaneous presence of NO_2 and NH_3, the PPy/rGO sensor response may be decreased due to the competition or complementarity between electron donors (NH_3) and electron acceptors (NO_2).

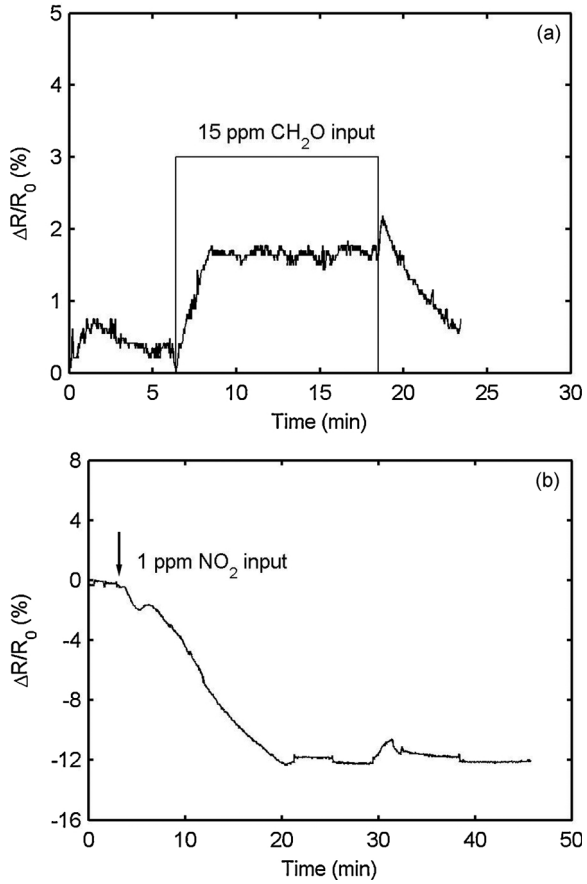


Fig. 6. The response of the PPy/rGO sensor in 50 % RH at 20 °C: (a) for 15 ppm formaldehyde (CH_2O) and (b) for 1 ppm nitride dioxide (NO_2).

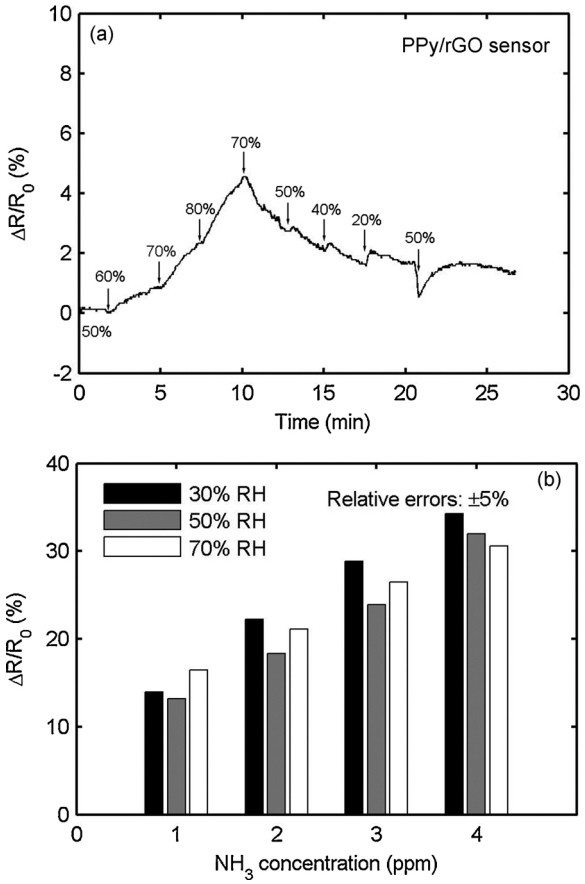


Fig. 7. (a) the response of the PPy/rGO sensor itself for humidity in the range from 20 % to 80 % at 20 °C; (b) the response of the PPy/rGO sensor exposed to NH_3 in the range from 1 to 4 ppm and at 30, 50 and 70 % RH.

3.4. Humidity influence

Humidity influence is an important factor for sensor application. We test the humidity influence on the response of the PPy/rGO sensor itself (NH_3 = 0 ppm). The measurements are carried out for a relative humidity (RH) range from 20 to 80 % at 20 °C, as shown in Fig. 7a. The humidity influence is quite small when the RH is lower than 80 %. Specifically, a change of 10 % RH brings a response of less than 0.8 % in average for the PPy/rGO sensor itself. We also test the humidity influence on the PPy/G sensor response in different concentration of NH_3. Fig. 7b plots the sensor response for NH_3 in the range from 1 to 4 ppm and at 30, 50 and 70 % RH. It can be seen that the variations of the sensor response is about ± 5 % between 30 and 70 % RH. For 1 ppm NH_3, a change of 10 % RH brings a response variation of 2.5 % in average. This value is 2.4 times smaller than the sensor sensitivity of 6.1 %/ppm in wet air. In general, water (H_2O) molecules can adsorb on the rGO through functional groups of C—OH, C—O—C and COOH. This should influence the sensor resistance by redistributing electrons in the rGO sheets. However, the PPy layer protects the rGO from H_2O molecules due to the PPy hydrophobic nature [56]. Yin et al. [57] reported that the detection capability of the PPy/rGO sensor is not severely affected by the relative humidity in the range from 0 to 80 % RH. In our case, the resistance of the PPy/rGO sensor itself is not sensitive to the RH in the range from 20 to 80 %. This implies that almost all the sensor surface is covered by the uniform and thin PPy layer. This also explains why the PPy/rGO sensor response only has weak variations when humidity is changed in the range from 30 to 70 % RH.

3.5. Reproducibility

Presently, the sensor reproducibility is an issue due to the fact that the size, thickness and uniformity of the GO dispersions are not well controlled. We tried 3 methods (in Supplementary material) for depositing GO dispersions (in water) on the IDEs, namely dropping, spraying, and ultrasonic spray pyrolysis. Even if the last one is the best among 3 methods, the distribution and size of the GO dispersions are still random. As can be seen in Fig. 1c, GO dispersions are agglomerated to form clusters with the lateral sizes from 500 nm up to several micrometer and the minimum thickness of about 3 nm. The local thickness of some clusters can reach 10 − 15 nm [45]. When the agglomerated cluster is thick enough to stack and form multiple rGO sheets, NH_3 molecules can only adsorb on the top layer of the rGO. In this case, electric current between the IDEs will pass through the bottom layer of the rGO. As a result, the sensor resistance cannot be completely modified by NH_3 molecules, degrading the sensor performance. This work presents a proof-of-principle sensor. For industrial production and commercial application, we will improve the conditions in ultrasonic spray pyrolysis or find the other deposition methods, such as inkjet.

3.6. Sensing mechanism and discussion

The sensing behaviours of the PPy/rGO sensor are attributed to the electron transfer between NH_3 molecule and the PPy/rGO composite [49]. On the one hand, as described by the following equations, the PPy polymer behaves like a *p*-type semiconductor [58,59]. When the electron-donating NH_3 molecules adsorb onto the PPy surface, electrons transfer from NH_3 to the π backbone of the PPy [60]. This neutralizes

holes in the PPy, thereby increasing the PPy resistance. For desorption, the electrons come back from the PPy to NH_3 and then the neutralized PPy becomes *p*-type, recovering the PPy resistance to its original value. The resistance change from the electron transfer occurring on the surface of the PPy can be effectively transferred to the IDEs through the rGO. It is worth noting that the electron transfer between the PPy and rGO is feasible due to the good interfacial affinity.

$$PPy + NH_3 \leftrightarrow PPy, NH_3 \text{ Adsorption} \quad (2)$$

$$PPy, NH_3 \leftrightarrow PPy + e, NH_3^+ \text{ Charge transfer} \quad (3)$$

On the other hand, the rGO includes a high density of sp^2-bonded carbons, vacancies, structural defects and residual oxygen groups. They build a hole-transporting matrix, which behaves as a p-type semiconductor. The adsorbed NH_3 may transfer to the rGO matrix through the ultrathin PPy layer, donating electrons to the rGO [61]. The electrons transfer depletes holes in the matrix, also increasing the rGO resistance [62]. The resistance change is directly measured between the IDEs.

The synergistic effect of the PPy and rGO can explain why the PPy/rGO sensor exhibits significantly higher sensitivity than the naked rGO sensor (as shown in Fig. 5d). Although pure PPy is a sensing material for NH_3 at room temperature, the response/recovery time is very long. The ultrathin PPy layer allows electrons to quickly transfer between NH_3 molecules and the PPy/rGO composite. Besides, the presence of the PPy molecules on the surface of the rGO allows the complete interaction between NH_3 and the binding sites. In other words, the adsorbed NH_3 molecules can bind on the rGO through the ultrathin PPy layer for the electron transfer. It can also be seen in Fig. 5 that the background noise of the PPy/rGO sensor is much lower than that of the naked rGO sensor, thanks to the ultrathin PPy layer. Therefore, the ultrathin PPy layer plays an important role in the PPy/rGO sensor response.

The sensitivity of the PPy/rGO sensor (6.1 %/ppm) is evidently higher than that of the PPy/G sensor (1.7 %/ppm) in our previous work. Presumably, the adsorbed NH_3 molecules bind not only onto low-energy sites (such as sp^2-bonded carbon), but also onto high-energy sites (such as vacancies, structural defects and oxygen functional groups) [38,39]. In the case of the PPy/G, NH_3 molecules can only adsorb onto sp^2-bonded carbon of the CVD graphene. Our results indicate that the fabrication of the gas sensors does not need high-quality graphene sheets and the rGO is a preferential material to obtain a large amount of defective graphene at low cost.

It is emphasized that our PPy/rGO sensor presents higher sensitivity than the same sensor fabricated by chemical oxidative polymerization [32]. This may be explained by the following fact. The residual oxygen groups in the rGO, mostly in the form of hydroxyl and epoxy groups, render it strongly hydrophilic and are reactive sites for the nucleation and growth of the PPy layer in electropolymerization. Therefore, electropolymerization is more effective synthesis of the PPy on the rGO compared to chemical oxidative polymerization.

4. Conclusions

In this study, we developed an ammonia (NH_3) sensor, in which an ultrathin polypyrrole (PPy) layer is synthesized on reduced graphene oxide (rGO) by electropolymerization. The thermal reduction of graphene oxide is confirmed by Raman and X-ray photoelectron spectroscopy. The morphology of the ultrathin PPy layer in terms of coverage on the rGO is observed by scanning electron microscopy and is supported by secondary ion mass spectrometry results. The sensor exhibits a linear response for NH_3 in the range from 1 to 4 ppm at room temperature, with a sensitivity of 6.1 %/ppm, response and recovery times of 1 and 5 min, respectively. The sensor is weakly affected by humidity and is specific for NH_3 towards interfering gases (CH_2O and H_2). These excellent performances are attributed to the synergistic effect of the PPy/rGO composite. The ultrathin PPy layer over the rGO directly reacts with NH_3. This simultaneously allows the NH_3 molecules to pass through and react with sp^2-bonded carbon atoms. Compared to CVD graphene, the rGO includes high density of vacancies, structural defects and oxygen functional groups. These enhance NH_3 adsorption, increasing the sensor sensitivity. The rGO sheets not only serve as a support material for the PPy electropolymerization, but also favour the electron transport, shortening the response/recovery time. Apart from that, the ultrathin PPy layer has hydrophobic nature, protecting the PPy/rGO sensor from humidity. It is the first time that the rGO is used as the support material for the PPy synthesis in electropolymerization. The post-step PPy electropolymerization is simple, low cost, and compatible with CMOS technology, as well as suitable for mass production. Our results indicate that the PPy electropolymerization is promising to manufacture NH_3 sensors. This research demonstrates a simple fabrication method of the NH_3 sensors with high performance and room-temperature operation. The present sensor is promising as a smart sensor and sensing system for different applications due to low price, low power consumption and scalable production. However, this work presents a proof-of-principle sensor. For industrial production and commercial application we will improve the sensor reproducibility.

Declaration of Competing Interest

The authors declare that they have no known competing financial interests or personal relationships that could have appeared to influence the work reported in this paper.

Acknowledgments

The authors would like to thank the staff of UCL's Winfab and Welcome for technical support, as well as Claude Poleunis for SIMS and Pierre Eloy for XPS measurements, respectively. They would also like to thank Miloud Zitout for sensors wire bonding. This work is financially supported by the Micro+ project co-funded by the European Regional Development Fund (ERDF) and Wallonia, Belgium (No. 675781-642409).

Appendix A. Supplementary data

Supplementary material related to this article can be found, in the online version, at doi:https://doi.org/10.1016/j.snb.2019.127423.

References

[1] L. Wang, H. Huang, S. Xiao, D. Cai, Y. Liu, B. Liu, D. Wang, C. Wang, H. Li, Y. Wang, Q. Li, T. Wang, Enhanced sensitivity and stability of room-temperature NH $_3$ sensors using core–shell CeO $_2$ nanoparticles@cross-linked PANI with p–n heterojunctions, ACS Appl. Mater. Interfaces 6 (2014) 14131–14140, https://doi.org/10.1021/am503286h.

[2] J. Wang, X. Wei, P. Wangyang, Gas-sensing devices based on Zn-doped NiO two-dimensional grainy films with fast response and recovery for ammonia molecule detection, Nanoscale Res. Lett. 10 (2015), https://doi.org/10.1186/s11671-015-1170-2.

[3] B. Timmer, W. Olthuis, A. van den Berg, Ammonia sensors and their applications—a review, Sens. Actuators B Chem. 107 (2005) 666–677, https://doi.org/10.1016/j.snb.2004.11.054.

[4] N.E. Agbor, J.P. Cresswell, M.C. Petty, A.P. Monkman, An optical gas sensor based on polyaniline Langmuir-Blodgett films, Sens. Actuators B Chem. 41 (1997) 137–141, https://doi.org/10.1016/S0925-4005(97)80286-9.

[5] T. Nagai, S. Tamura, N. Imanaka, Solid electrolyte type NH3 gas sensor applicable in a humid atmosphere, Electrochemistry 78 (2010) 126–128, https://doi.org/10.5796/electrochemistry.78.126.

[6] Y.C. Lee, H. Huang, O.K. Tan, M.S. Tse, Semiconductor gas sensor based on Pd-doped SnO2 nanorod thin films, Sens. Actuators B Chem. 132 (2008) 239–242, https://doi.org/10.1016/j.snb.2008.01.028.

[7] A. Yimit, K. Itoh, M. Murabayashi, Detection of ammonia in the ppt range based on a composite optical waveguide pH sensor, Sens. Actuators B Chem. 88 (2003) 239–245, https://doi.org/10.1016/S0925-4005(02)00324-6.

[8] G.H. Mount, B. Rumburg, J. Havig, B. Lamb, H. Westberg, D. Yonge, K. Johnson, R. Kincaid, Measurement of atmospheric ammonia at a dairy using differential optical absorption spectroscopy in the mid-ultraviolet, Atmos. Environ. 36 (2002) 1799–1810, https://doi.org/10.1016/S1352-2310(02)00158-9.

[9] J. Janata, M. Josowicz, Organic semiconductors in potentiometric gas sensors, J. Solid State Electrochem. 13 (2009) 41–49, https://doi.org/10.1007/s10008-008-0597-0.

[10] L. Aba, Y. Yusuf, Mitrayana, D. Siswanta, Junaidi, K. Triyana, Sensitivity improvement of Ammonia gas sensor based on poly(3,4-ethylenedioxythiophene):poly (styrenesulfonate) by employing doping of Bromocresol Green, J. Nanotechnol. 2014 (2014) 1–5, https://doi.org/10.1155/2014/864274.

[11] H.-I. Chen, C.-Y. Hsiao, W.-C. Chen, C.-H. Chang, T.-C. Chou, I.-P. Liu, K.-W. Lin, W.-C. Liu, Characteristics of a Pt/NiO thin film-based ammonia gas sensor, Sens. Actuators B Chem. 256 (2018) 962–967, https://doi.org/10.1016/j.snb.2017.10.032.

[12] N. Chartuprayoon, C.M. Hangarter, Y. Rheem, H. Jung, N.V. Myung, Wafer-scale fabrication of single polypyrrole nanoribbon-based ammonia sensor, J. Phys. Chem. C 114 (2010) 11103–11108, https://doi.org/10.1021/jp102858w.

[13] M.-Z. Dai, Y.-L. Lin, H.-C. Lin, H.-W. Zan, K.-T. Chang, H.-F. Meng, J.-W. Liao, M.-J. Tsai, H. Cheng, Highly sensitive ammonia sensor with organic vertical nanojunctions for noninvasive detection of hepatic injury, Anal. Chem. 85 (2013) 3110–3117, https://doi.org/10.1021/ac303100k.

[14] A.T. Güntner, M. Righettoni, S.E. Pratsinis, Selective sensing of NH 3 by Si-doped α-MoO 3 for breath analysis, Sens. Actuators B Chem. 223 (2016) 266–273, https://doi.org/10.1016/j.snb.2015.09.094.

[15] M. D'Arienzo, L. Armelao, C.M. Mari, S. Polizzi, R. Ruffo, R. Scotti, F. Morazzoni, Macroporous WO_3 thin films active in NH_3 sensing: role of the gosted Cr isolated centers and Pt nanoclusters, J. Am. Chem. Soc. 133 (2011) 5296–5304, https://doi.org/10.1021/ja109511a.

[16] L. Wang, Z. Lou, T. Fei, T. Zhang, Templating synthesis of ZnO hollow nanospheres loaded with Au nanoparticles and their enhanced gas sensing properties, J. Mater. Chem. 22 (2012) 4767, https://doi.org/10.1039/c2jm15342d.

[17] S. Elouali, L.G. Bloor, R. Binions, I.P. Parkin, C.J. Carmalt, J.A. Darr, Gas sensing with nano-indium oxides (In_2O_3) prepared via continuous hydrothermal flow synthesis, Langmuir. 28 (2012) 1879–1885, https://doi.org/10.1021/la203565h.

[18] F. Schedin, A.K. Geim, S.V. Morozov, E.W. Hill, P. Blake, M.I. Katsnelson, K.S. Novoselov, Detection of individual gas molecules adsorbed on graphene, Nat. Mater. 6 (2007) 652–655, https://doi.org/10.1038/nmat1967.

[19] W.S. Hummers Jr, R. Offeman, Preparation of graphitic oxide, J. Am. Chem. Soc. 80 (1958) 1339.

[20] S. Zhang, H.-S. Chen, P. Yang, ZnO nanoflowers with single crystal structure towards enhanced gas sensing and photocatalysis, Phys. Chem. Chem. Phys. 17 (2019) 30300–30306.

[21] Y. Yang, S. Li, W. Yang, W. Yuan, J. Xu, Y. Jiang, In situ polymerization deposition of porous conducting polymer on reduced graphene oxide for gas sensor, ACS Appl. Mater. Interfaces 6 (2014) 13807–13814, https://doi.org/10.1021/am5032456.

[22] William S. Hummers, Richard E. Offeman, Preparation of graphitic oxide", March 20, J. Am. Chem. Soc. 80 (6) (1958) 1339, https://doi.org/10.1021/ja01539a017.

[23] Y. Xu, G. Shi, Assembly of chemically modified graphene: methods and applications, J. Mater. Chem. 21 (2011) 3311–3323, https://doi.org/10.1039/C0JM02319A.

[24] X. Wang, H. Bai, G. Shi, Size fractionation of graphene oxide sheets by pH-assisted selective sedimentation, J. Am. Chem. Soc. 133 (2011) 6338–6342, https://doi.org/10.1021/ja200218y.

[25] L. Al-Mashat, K. Shin, K. Kalantar-zadeh, J.D. Plessis, S.H. Han, R.W. Kojima, R.B. Kaner, D. Li, X. Gou, S.J. Ippolito, W. Wlodarski, Graphene/polyaniline nanocomposite for hydrogen sensing, J. Phys. Chem. C 114 (2010) 16168–16173, https://doi.org/10.1021/jp103134u.

[26] S. Carquigny, J. Sanchez, F. Berger, B. Lakard, F. Lallemand, Ammonia gas sensor based on electrosynthesized polypyrrole films, Talanta 78 (2009) 199–206, https://doi.org/10.1016/j.talanta.2008.10.056.

[27] T. Patois, J.-B. Sanchez, F. Berger, J.-Y. Rauch, P. Fievet, B. Lakard, Ammonia gas sensors based on polypyrrole films: influence of electrodeposition parameters, Sens. Actuators B Chem. 171–172 (2012) 431–439, https://doi.org/10.1016/j.snb.2012.05.005.

[28] J. Qi, X. Xu, X. Liu, K.T. Lau, Fabrication of textile based conductometric polyaniline gas sensor, Sens. Actuators B Chem. 202 (2014) 732–740, https://doi.org/10.1016/j.snb.2014.05.138.

[29] T. Hibbard, K. Crowley, F. Kelly, F. Ward, J. Holian, A. Watson, A.J. Killard, Point of care monitoring of hemodialysis patients with a breath Ammonia measurement device based on printed polyaniline nanoparticle sensors, Anal. Chem. 85 (2013) 12158–12165, https://doi.org/10.1021/ac403472d.

[30] C. Xiang, D. Jiang, Y. Zou, H. Chu, S. Qiu, H. Zhang, F. Xu, L. Sun, L. Zheng, Ammonia sensor based on polypyrrole–graphene nanocomposite decorated with titania nanoparticles, Ceram. Int. 41 (2015) 6432–6438, https://doi.org/10.1016/j.ceramint.2015.01.081.

[31] X. Tang, D. Lahem, J.-P. Raskin, P. Gerard, X. Geng, N. Andre, M. Debliquy, A fast and room-temperature operation Ammonia sensor based on compound of graphene with polypyrrole, IEEE Sens. J. 18 (2018) 9088–9096, https://doi.org/10.1109/JSEN.2018.2869203.

[32] D.C. Tiwari, P. Atri, R. Sharma, Sensitive detection of ammonia by reduced graphene oxide/polypyrrole nanocomposites, Synth. Met. 203 (2015) 228–234, https://doi.org/10.1016/j.synthmet.2015.02.026.

[33] S. Bai, Y. Zhao, J. Sun, Y. Tian, R. Luo, D. Li, A. Chen, Ultrasensitive Room Temperature NH3 Sensor Based on Graphene-Polyaniline Hybrid Loading on PET Thin Film, (2012), p. 5.

[34] Y. Wang, L. Zhang, N. Hu, Y. Wang, Y. Zhang, Z. Zhou, Y. Liu, S. Shen, C. Peng, Ammonia gas sensors based on chemically reduced graphene oxide sheets self-assembled on Au electrodes, Nanoscale Res. Lett. 9 (2014), https://doi.org/10.1186/1556-276X-9-251.

[35] T.N. Ly, S. Park, Highly sensitive ammonia sensor for diagnostic purpose using reduced graphene oxide and conductive polymer, Sci. Rep. 8 (2018), https://doi.org/10.1038/s41598-018-36468-z.

[36] N. Hu, Z. Yang, Y. Wang, L. Zhang, Y. Wang, X. Huang, H. Wei, L. Wei, Y. Zhang, Ultrafast and sensitive room temperature NH_3 gas sensors based on chemically reduced graphene oxide, Nanotechnology 25 (2014) 025502, , https://doi.org/10.1088/0957-4484/25/2/025502.

[37] X. Huang, N. Hu, L. Zhang, L. Wei, H. Wei, Y. Zhang, The NH3 sensing properties of gas sensors based on aniline reduced graphene oxide, Synth. Met. 185–186 (2013) 25–30, https://doi.org/10.1016/j.synthmet.2013.09.034.

[38] C. Wang, S. Lei, X. Li, S. Guo, P. Cui, X. Wei, W. Liu, H. Liu, A reduced GO-Graphene hybrid gas sensor for ultra-low concentration ammonia detection, Sensors 18 (2018) 3147, https://doi.org/10.3390/s18093147.

[39] I. Karaduman, E. Er, H. Çelikkan, N. Erk, S. Acar, Room-temperature ammonia gas sensor based on reduced graphene oxide nanocomposites decorated by Ag, Au and Pt nanoparticles, J. Alloys Compd. 722 (2017) 569–578, https://doi.org/10.1016/j.jallcom.2017.06.152.

[40] Z. Ye, H. Tai, R. Guo, Z. Yuan, C. Liu, Y. Su, Z. Chen, Y. Jiang, Excellent ammonia sensing performance of gas sensor based on graphene/titanium dioxide hybrid with improved morphology, Appl. Surf. Sci. 419 (2017) 84–90, https://doi.org/10.1016/j.apsusc.2017.03.251.

[41] H. Tai, Z. Yuan, W. Zheng, Z. Ye, C. Liu, X. Du, ZnO nanoparticles/reduced graphene oxide bilayer thin films for improved NH3-sensing performances at room temperature, Nanoscale Res. Lett. 11 (2016), https://doi.org/10.1186/s11671-016-1343-7.

[42] X. Huang, N. Hu, R. Gao, Y. Yu, Y. Wang, Z. Yang, E. Siu-Wai Kong, H. Wei, Y. Zhang, Reduced graphene oxide–polyaniline hybrid: preparation, characterization and its applications for ammonia gas sensing, J. Mater. Chem. 22 (2012) 22488, https://doi.org/10.1039/c2jm34340a.

[43] Y. Qin, B. Zhang, Z. Zhang, Combination of PPy with three-dimensional rGO to construct bioinspired nanocomposite for NH3-sensing enhancement, Org. Electron. 70 (2019) 240–245, https://doi.org/10.1016/j.orgel.2019.04.023.

[44] U. Hashim, R. Adzhri, M.K.M. Arshad, M.F.M. Fathil, A.R. Ruslinda, R.M. Ayub, M.N.M. Nuzaihan, A.H. Azman, M. Zaki, A.B. Suriani, Spray pyrolysis of graphene oxide for field-effect transistor biosensor application, 2015 2nd International Conference on Biomedical Engineering (ICoBE), IEEE, Penang, Malaysia, 2015, pp. 1–4, , https://doi.org/10.1109/ICoBE.2015.7235909.

[45] O.M. Slobodian, Yu.S. Milovanov, V.A. Skryshevsky, A.V. Vasin, X. Tang, J.-P. Raskin, P.M. Lytvyn, K.V. Svezhentsova, S.V. Malyuta, A.N. Nazarov, Reduced graphene oxide obtained using the spray pyrolysis technique for gas sensing, Semicond. Phys. Quantum Electron. Optoelectron. 22 (2019) 98–103, https://doi.org/10.15407/spqeo22.01.098.

[46] X. Tang, J.-P. Raskin, D. Lahem, A. Krumpmann, A. Decroly, M. Debliquy, A formaldehyde sensor based on molecularly-imprinted polymer on a TiO2 nanotube array, Sensors 17 (2017) 675, https://doi.org/10.3390/s17040675.

[47] A.C. Ferrari, Raman spectroscopy of graphene and graphite: disorder, electron–phonon coupling, doping and nonadiabatic effects, Solid State Commun. 143 (2007) 47–57, https://doi.org/10.1016/j.ssc.2007.03.052.

[48] L.M. Malard, M.A. Pimenta, G. Dresselhaus, M.S. Dresselhaus, Raman spectroscopy in graphene, Phys. Rep. 473 (2009) 51–87, https://doi.org/10.1016/j.physrep.2009.02.003.

[49] A.C. Ferrari, J. Robertson, Interpretation of Raman spectra of disordered and amorphous carbon, Phys. Rev. B 61 (2000) 14095–14107, https://doi.org/10.1103/PhysRevB.61.14095.

[50] G. Sobon, J. Sotor, J. Jagiello, R. Kozinski, M. Zdrojek, M. Holdynski, P. Paletko, J. Boguslawski, L. Lipinska, K.M. Abramski, Graphene oxide vs reduced graphene oxide as saturable absorbers for Er-doped passively mode-locked fiber laser, Opt. Express 20 (2012) 19463, https://doi.org/10.1364/OE.20.019463.

[51] O. Akhavan, E. Ghaderi, Escherichia coli bacteria reduce graphene oxide to bactericidal graphene in a self-limiting manner, Carbon 50 (2012) 1853–1860, https://doi.org/10.1016/j.carbon.2011.12.035.

[52] Y. Guo, X. Sun, Y. Liu, W. Wang, H. Qiu, J. Gao, One pot preparation of reduced graphene oxide (RGO) or Au (Ag) nanoparticle-RGO hybrids using chitosan as a reducing and stabilizing agent and their use in methanol electrooxidation, Carbon 50 (2012) 2513–2523, https://doi.org/10.1016/j.carbon.2012.01.074.

[53] N. Kumar, A.K. Srivastava, H.S. Patel, B.K. Gupta, G.D. Varma, Facile synthesis of ZnO-reduced graphene oxide nanocomposites for NO_2 gas sensing applications: facile synthesis of ZnO-reduced graphene oxide nanocomposites, Eur. J. Inorg. Chem. 2015 (2015) 1912–1923, https://doi.org/10.1002/ejic.201403172.

[54] C. Peng, J. Guo, W. Yang, C. Shi, M. Liu, Y. Zheng, J. Xu, P. Chen, T. Huang, Y. Yang, Synthesis of three-dimensional flower-like hierarchical ZnO nanostructure and its enhanced acetone gas sensing properties, J. Alloys Compd. 654 (2016) 371–378, https://doi.org/10.1016/j.jallcom.2015.09.120.

[55] X. Tang, P.-A. Haddad, N. Mager, X. Geng, N. Reckinger, S. Hermans, M. Debliquy, J.-P. Raskin, Chemically deposited palladium nanoparticles on graphene for hydrogen sensor applications, Sci. Rep. 9 (2019), https://doi.org/10.1038/s41598-019-40257-7.

[56] D. Jung, M. Han, G.S. Lee, Humidity-sensing characteristics of multi-walled carbon nanotube sheet, Mater. Lett. 122 (2014) 281–284, https://doi.org/10.1016/j.matlet.2014.02.049.

[57] Y. Yin, H. Zhang, P. Huang, C. Xiang, Y. Zou, F. Xu, L. Sun, Inducement of nanoscale Cu–BTC on nanocomposite of PPy–rGO and its performance in ammonia sensing, Mater. Res. Bull. 99 (2018) 152–160, https://doi.org/10.1016/j.materresbull.2017.11.012.

[58] M. Bazzaoui, J.I. Martins, E. Machnikova, E.A. Bazzaoui, L. Martins, Polypyrrole films electrosynthesized on stainless steel grid from saccharinate aqueous solution

and its behaviour toward acetone vapor, Eur. Polym. J. 43 (2007) 1347–1358, https://doi.org/10.1016/j.eurpolymj.2007.01.013.
[59] D. Blackwood, M. Josowicz, Work function and spectroscopic studies of interactions between conducting polymers and organic vapors, J. Phys. Chem. 95 (1991) 493–502, https://doi.org/10.1021/j100154a086.
[60] A. Joshi, S.A. Gangal, S.K. Gupta, Ammonia sensing properties of polypyrrole thin films at room temperature, Sens. Actuators B Chem. 156 (2011) 938–942, https://doi.org/10.1016/j.snb.2011.03.009.
[61] O. Leenaerts, B. Partoens, F.M. Peeters, Adsorption of H 2 O, N H 3, CO, N O 2, and NO on graphene: a first-principles study, Phys. Rev. B 77 (2008), https://doi.org/10.1103/PhysRevB.77.125416.
[62] R. Ghosh, A. Midya, S. Santra, S.K. Ray, P.K. Guha, Chemically reduced graphene oxide for Ammonia detection at room temperature, ACS Appl. Mater. Interfaces 5 (2013) 7599–7603, https://doi.org/10.1021/am4019109.



Xiaohui Tang received the Ph. D. degree in Applied Sciences from Université Catholique de Louvain, Belgium in 2001. From 1983 to 1994, she worked at Kunming Institute of Physics, China. She then was a free researcher at IMEC, Leuven, Belgium in 1995. Presently, she is working at ICTEAM institute, Université catholique de Louvain, Belgium as a Senior Research. She has more 130 publications in international journals and conferences, 5 book chapters and 5 patents. Her current interest is in fabrication and characterization gas sensors and smart prototypes.



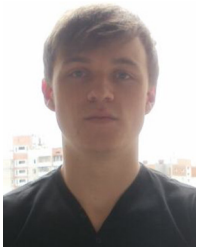
Jean-Pierre Raskin (IEEE M'97, IEEE SM'06, IEEE F'14) was born in Aye, Belgium, in 1971. He received the Industrial Engineer degree from the Institut Supérieur Industriel d'Arlon, Belgium, in 1993, and the M.S. and Ph.D. degrees in Applied Sciences from the Université catholique de Louvain (UCLouvain), Louvain-la-Neuve, Belgium, in 1994 and 1997, respectively. From 1994 to 1997, he was a Research Engineer at the Microwave Laboratory, UCLouvain, Belgium. He worked on the modeling, characterization and fabrication of MMIC's in Silicon-on-Insulator (SOI) technology for low-power, low-voltage applications. In 1998, he joined the EECS Department of The University of Michigan, Ann Arbor, USA. He has been involved in the development and characterization of micromachining fabrication techniques for microwave and millimeter-wave circuits and microelectromechanical transducers/amplifiers working in harsh environments. In 2000, he joined the Microwave Laboratory of UCLouvain, Louvain-la-Neuve, Belgium, as Associate Professor, and he has been a Full Professor since 2007. From September 2009 to September 2010, he was visiting professor at Newcastle University, Newcastle Upon Tyne, UK. He was the head of the Electrical Engineering Department of UCLouvain between 2014 and 2017. His research interests are the modeling, wideband characterization and fabrication of advanced SOI MOSFETs as well as micro and nanofabrication of MEMS / NEMS sensors and actuators, including the extraction of intrinsic material properties at nanometer scale. He is IEEE Fellow, EuMA Associate Member, Société de l'électricité, de l'électronique et des technologies de l'information et de la communication (SEE) Member, and Material Research Society (MRS) Member. He was the recipient of the Médaille BLONDEL 2015, famous French reward that honors each year a researcher for outstanding advances in science which have demonstrated a major impact in the electrical and electronics industry. He received the SOI Consortium Award 2016 and the European SEMI Award 2017 in recognition in his vision and pioneering work for RF SOI. In 2017, he received with the NGO Louvain Cooperation the prestigious European Global Education Innovation Award. He is author or co-author of more than 350 scientific journal articles.



Nadzeya Kryvutsa was born in Vitebsk (Belarus) in 1989. She obtained a Master degree in Chemical Sciences from the Université catholique de Louvain (UCL, Belgium) in 2014. She started a PhD thesis at the same year at Institute of Condensed Matter and Nanosciences (IMCN) in co-promotion within the laboratory of Professor S. Hermans and the laboratory of Professor B. Hackens. The field of her research is functionalization of single-layer graphene by magnetic nanoparticles and study of electronic and transport properties of modified graphene. She is also a teaching assistant at UCL.



Sophie Hermans is an Inorganic Chemist. She obtained her first degree ('Licence en Chimie') at UCLouvain in Belgium, with final-year and DEA projects supervised by Prof. M. Devillers. She started her research career as a synthetic chemist, making new metal complexes, and in particular mixed-metal clusters. She obtained her PhD at the University of Cambridge (UK) under the supervision of Prof. Brian F. G. Johnson. She obtained a Junior Research Fellowship (Newnham College) to pursue postdoctoral studies in Cambridge and collaborated with Prof. Sir John M. Thomas to immobilize the mixed-metal clusters in MCM-41 for heterogeneous catalytic applications. After moving back to UCLouvain with a FNRS 'Chargée de recherches' post, she started working on carbon-supported catalysts and chemical functionalization of (nano)carbon surfaces. She obtained the FNRS 'Chercheur Qualifié' and Assistant Professor positions in 2005 and since then was promoted to Full Professor in 2014 and FNRS 'Maître de recherches' in 2015. Her research interests are still in connection with inorganic molecular chemistry, carbon materials, surface functionalization and nanostructured materials preparation.



Oleksandr Slobodian junior research scientist of department of the Functional Materials and Nanostructures, V. Lashkaryov Institute of Semiconductor Physics NAS of Ukraine. The area of scientific interests includes investigation of electrical, optical and sensors properties of graphene and ultrathin carbon films.



Nazarov A. Nazarov Doctor of Sciences in Physics and Mathematics, Head of department of the Functional Materials and Nanostructures, V. Lashkaryov Institute of Semiconductor Physics, NAS of Ukraine, Professor of department of General Physics and Solid State Physics, National Technical University of Ukraine "Igor Sikorsky KPI". The area of scientific interests of Dr. Nazarov includes physics, technology and characterization of nanoscaled carbon based materials and devices, SOI structures and devices, radiation effects in carbon and silicon based materials, structures and devices.



Marc Debliquy received his Ph.D. at Faculty of Engineering in Mons (Belgium) in1999 in the field of organic semiconductors for fire detection. He joined the Sochinor Company in 2000. He left in 2003 for joining Materia Nova. He was responsible for the research activities in the field of gas sensors. Since October 2008, he joined the Material Science Department of Faculty of Engineering of University of Mons and worked as a team leader of semiconductor and sensor group. He was promoted as associate professor in September 2013. His main research interest is smart coatings for chemical detection. He is also co-founder of the spin off company B-Sens specialized in optical fiber sensors.